JOURNAL OF APPLIED ELECTROCHEMISTRY **28** (1998) 781–789

Influence of electrolyte impurities on current efficiency in aluminium electrolysis cells

Å. STERTEN

The Department of Electrochemistry, Norwegian University of Science and Technology, 7034 Trondheim, Norway

P. A. SOLLI

Hydro Aluminium, Årdal Metal Plant, PO Box 303, 5870 Øvre Årdal, Norway

E. SKYBAKMOEN

SINTEF Materials Technology, 7034 Trondheim, Norway

Received 12 December 1996; 7 September 1997

The influence of electrolyte impurity species on current efficiency with respect to aluminium (CE) was studied in a specially designed laboratory cell at 980 °C, with a graphite anode and a cathodic current density of 0.85 A cm^{-2}. The electrowinning was performed in a base melt of Na_3AlF_6 with a NaF/AlF_3 molar ratio of 2.5 and with 4–6 wt % Al_2O_3 and 5 wt % CaF_2. Impurity species, probably present in only one valence state in the electrolyte, Mg, Ba and B, had no measurable effect on CE for low impurity concentrations. Sn, added to the electrolyte as SnO_2, also did not affect current efficiency, probably due to its low solubility. The results show a linear decrease in CE with increasing electrolyte concentration of the polyvalent impurity species from the elements, Fe, P, V, Si, Zn, Ti and Ga. The decrease was found to be within the range 0.1 to 0.7% in CE per 0.01 wt % of impurity cations present in the electrolyte, with phosphorus ions as the most detrimental. The effects of the individual impurity species on CE appear to be roughly additive for electrolytes containing more than one impurity species. The results obtained cannot be explained by a simple codeposition mechanism or a single reduction to a soluble species of a lower valency. The most likely mechanism explaining the observed decrease in CE for a large number of impurity species is cyclic redox reactions in the cathode and anode/CO_2 interfacial boundary layers. Such a mechanism may also be the dominant one in commercial cells, since the impurity levels are of the same size as in the laboratory cell.

Keywords: *aluminium*, *current efficiency*, *impurity species*

List of symbols

B_i	proportionality constant (Equations 18 and 19)
c_i	concentration (mass percent)
c_M	total concentration of impurity element M (mass percent)
Δc_{imp}	concentration change of impurity species (mol cm^{-3})
C'	proportionality constant
D_{imp}	diffusion coefficient of an impurity element (cm^2 s^{-1})
D_{mix}	total or a 'mixed' diffusion coefficient of reduced entities (cm^2 s^{-1})
F	Faraday constant (C mol^{-1})
i_{Al}	local current density for the aluminium deposition reaction (A cm^{-2})
i_{loss}	local current density for all cathodic side reactions (A cm^{-2})
i_c	local cathodic current density (A cm^{-2})
J_i	local mass flux density of component i (mol cm^{-2} s^{-1})
k_i	local mass transfer coefficient of component i (cm s^{-1})
k_{mix}	local mixed mass transfer coefficient (or standard rate constant) of all cathodic side reactions (mol cm^{-2} s^{-1})
x	coordinate axis (cm)
x_i	molar fraction of component i
z	valence change in redox reactions

Greek letters

δ	total cathode boundary layer thickness (cm)
δ_{imp}	thickness of the 'impurity diffusion layer' (cm)
δ_{mix}	thickness of the diffusion layer of reduced entities (cm)
ε	local current efficiency for the aluminium deposition reaction (%)
ε_{max}	current efficiency limit for a defined rate determining step (%)
η	concentration overpotential/polarization (V)

0021-891X

1. Introduction

A detailed description of the processes in aluminium electrolysis cells determining the current efficiency with respect to aluminium (CE) was given previously [1], and a model describing the local CE was developed [2]. A special laboratory cell was designed and tested [3], and CE as a function of temperature, electrolyte composition and current density was studied, and CE model parameters were derived [4].

Electrolytes in commercial Hall–Héroult cells always contain impurities which are introduced to the electrolyte through alumina feeding, carbon anode consumption, use of tools etc. The structure of impurities dissolved in cryolite-based melts is essentially unknown, so they will simply be treated as uncomplexed ionic species. Johansen [5] found that iron contaminants in the electrolyte consisted of both Fe^{2+} and Fe^{3+} species ($\sim$70% Fe^{2+}). In addition commercial electrolytes contain several other impurity species, for example, phosphorous, silicon, vanadium, titanium, chromium, nickel, copper, cadmium and gallium [6–15].

Considerable decrease in CE by small additions of various impurity species (P, V, Ti, Fe, Ga and Si species) was found in laboratory cells [10–14]. Szeker [10] ascribed the losses in CE to cyclic redox reactions involving reoxidation of impurities by air. A similar explanation was proposed by Kerouanton and Badoz–Lambling [11] who suggested that elemental P was reoxidized to P_2O_5 by air, and then fell into the electrolyte after having been condensed on the inside of the furnace lining. Frolova *et al.* [12] proposed that a considerable part of the reduction in CE when adding P_2O_5 to the electrolyte could be ascribed to an increase in the electrolyte temperature, giving a higher content of carbon dust in the bulk electrolyte followed by an increase in the ohmic resistance. Gerlach and Deininger [13] proposed that cyclic redox reactions between P^{5+} and P^{3+} occurred at low concentrations, and between P^{5+}/P^{3+} and zero-valent P at higher concentrations. The other species (Fe, V and Ti) were assumed to be reduced only once, that is, not by a cyclic redox mechanism. Grjotheim *et al.* [7] discussed literature data and concluded that some kind of cyclic redox mechanism may play an important role when it comes to the deleterious effect of phosphorous and some other impurity species on CE. Keller [15] disregarded the possibility of iron existing as both di- and tri-valent species in the electrolyte, and claimed that the cyclic redox reactions involved cathodic reduction to metallic iron, a part of which was not alloyed with the aluminium, but instead transported towards the anode and reoxidized, that is, a cyclic mechanism involving Fe^{3+} and Fe.

Impurity species in the electrolyte may participate in various types of redox reactions. Species with only one valence state, can participate in simple cathodic deposition reactions. It can be stated that the effect of such a mechanism on CE is only of minor importance as long as the impurity concentrations are small. Impurities present in more than one oxidation state, must be assumed to take part in cyclic redox reactions [1]. Such impurities will have a marked detrimental effect on CE, as shown below. The theoretical analysis, described by Sterten and Solli [1], revealed that CE in commercial cells was partly determined by cyclic redox reactions in the cathode and anode boundary layers when polyvalent impurities are present in the electrolyte. The aim of the present work was (a) to establish reliable CE data and (b) to develop a simplified CE model describing the influence of impurities and derivation of model parameters.

2. Theory

2.1. *Chemical description of the effect of impurities on CE*

As discussed elsewhere [1] the cathodic side reactions giving rise to loss in CE can be described by the formation of reduced entities (RE), both monovalent aluminium (AlF_2^-),

$$Na^+ + AlF_3 + 2e^- = AlF_2^- + NaF \qquad (1)$$

and sodium dissolved in the electrolyte,

$$Na^+ + e^- = Na \qquad (2)$$

Dissolved sodium is in equilibrium with localized electrons [1], the cathodic formation of which tentatively may be written as

$$e^- = e' \qquad (3)$$

Localized electrons, e′, the origin of electronic conductivity in cryolite-based melts, play an important role for current inefficiency both in commercial and laboratory cells.

The description below is based on the assumption that there are no concentration gradients in the bulk of the electrolyte phase. It is further assumed that there is a steady state concentration level of several impurities in the electrolyte as usually is the case in commercial cells. This means that the equilibrium concentrations of RE (including e′) in the bulk electrolyte must be very low, since reactions between RE and impurities are likely to occur inside the cathode boundary layer, that is,

$$M^{(x+z)+} + ze' = M^{x+} \qquad (4)$$

where the impurity species M is present in the electrolyte in two oxidation states, $M^{(x+z)+}$ and M^{x+}. The concentration gradients in the cathode diffusion layer are illustrated in terms of linear gradients in Fig. 1, while Reaction 4 proceeds in a plane A at a certain distance from the metal surface. If the impurity level in the electrolyte is raised, as indicated by the stippled line in the figure, then the reaction plane, A, is moved towards the electrode surface, the net result being steeper concentration gradients and increasing loss of CE.

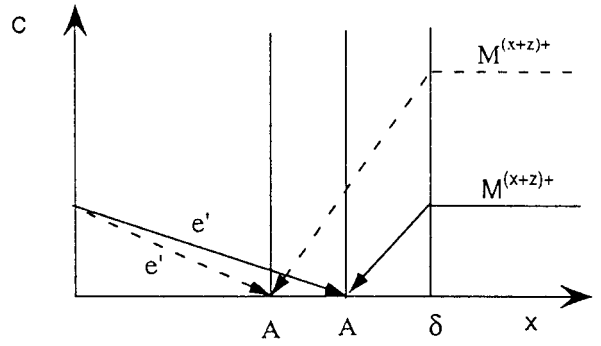

Fig. 1. Schematic concentration profiles of e′ and of reducible polyvalent impurity species, $M^{(x+z)+}$, in a cathode boundary layer of thickness δ, for two different impurity concentrations. The distance from the cathode is denoted x, and the planes of reaction are denoted A.

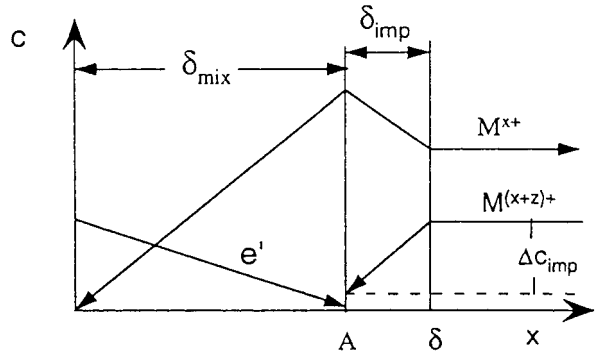

Fig. 2. Concentration profiles of impurities and e′ in the cathode boundary layer with a thickness δ. The distance from the aluminium cathode is denoted x. The plane of reaction, denoted A, separates the boundary layer in two distinct regions so that, $\delta = \delta_{mix} + \delta_{imp}$.

The process of cyclic redox reactions involves reduction of impurity species, mass transport, and reoxidation of impurity species with CO_2 as elsewhere discussed in detail [1, 2]. One impurity species may participate in a series of redox cycles, reacting with RE several times before being cathodically deposited and alloyed with the aluminium metal. The rate limiting steps, suitable for modelling, are supposed to be the mass transport of RE from the metal surface to the reaction plane A (see Fig. 1) and the mass transport of polyvalent impurities from the bulk electrolyte to the same plane A. (It is supposed that the reactions in plane A do not represent rate determining steps.)

2.2. *Modelling of CE*

As discussed elsewhere [2], the CE (ε) depends on several parameters,

$$\varepsilon = f(i_{Al}, i_{loss}) = f(x_{NaF}, x_{AlF_3}, x_1, x_2, \ldots, x_n, T, k_{NaF}, k_{mix}, \eta) \quad (5)$$

where i_{Al} and i_{loss} are the local current densities for the aluminium deposition reaction and for all cathodic loss reactions, respectively. $x_1, x_2, \ldots x_n$ are electrolyte additives including impurities with fixed concentrations. k_{NaF} and k_{mix} are local mass transfer coefficients and η is the overvoltage related to the aluminium deposition reaction.

The derivation given below is based on fixed parameters referred to Equation 5, independent of minor changes in the impurity concentrations. It should be emphasized that i_{Al} and i_{loss} will vary with impurity concentrations, but not their sum, which equals the local overall cathode current density, i_c. Fig. 2 illustrates idealized concentration profiles for RE represented by e′ and for M as impurity species.

The current density of side reactions corresponding to the profile where the plane A (Figs 1 and 2) approaches the total thickness of the diffusion layer, δ, is denoted $i_{loss,min}$, and may tentatively be described by Equation 6:

$$i_{loss,min} = C' \frac{D_{mix}}{\delta} \quad (6)$$

where C' is a constant and D_{mix} is a total or a 'mixed' diffusion coefficient of RE (including e′). This loss corresponds to the lowest impurity concentration necessary to establish cyclic redox reactions as a rate limiting process. If the impurity concentration decreases below this critical value, then RE will enter the bulk electrolyte phase [1], and a shift in the rate limiting steps will occur. The reduction of added impurities in such a case, partly to the metallic state, has been discussed elsewhere [1, 2].

An arbitrary, steady state impurity concentration level in the bulk may correspond to the concentration profiles given in Fig. 2, from which a general equation for the partial current density of side reactions may be derived:

$$i_{loss} = C' \frac{D_{mix}}{\delta_{mix}} \quad (7)$$

where δ in Equation 6 has been substituted by δ_{mix}. The mass transfer coefficient, k_{mix}, in Equation 5 is equal to the ratio D_{mix}/δ_{mix}. At the reaction site A in Fig. 2, the flux of RE from the cathode surface, J_{loss}, is roughly equal to the total flux of the reducible polyvalent impurity, J_{imp},

$$J_{loss} = J_{imp} \quad (8)$$

Then, it follows that

$$i_{loss} = C' \frac{D_{mix}}{\delta_{mix}} = zF \frac{D_{imp}}{\delta_{imp}} \Delta c_{imp} \quad (9)$$

where all symbols are as stated at the outset.

Rearrangement of Equation 9 gives

$$\delta_{mix} = \frac{C' D_{mix}(\delta - \delta_{mix})}{zF D_{imp} \Delta c_{imp}} \quad (10)$$

where δ_{imp} is

$$\delta_{imp} = \delta - \delta_{mix} \quad (11)$$

Introducing the term A' as

$$A' = \frac{C' D_{mix}}{zF D_{imp} \Delta c_{imp}} \quad (12)$$

in Equation 10, and solving for δ_{mix} gives

$$\delta_{mix} = \frac{A'\delta}{1 + A'} \quad (13)$$

Equation 9 is combined with Equation 13 as follows:

$$i_{loss} = C' \frac{D_{mix}}{\delta_{mix}} = C' D_{mix} \frac{(1 + A')}{\delta A'} \quad (14)$$

The Equations 14, 12 and 6 can be rearranged to give

$$i_{loss} = i_{loss,min} + \frac{zFD_{imp}}{\delta} \Delta c_{imp} \quad (15)$$

Current efficiency can then be expressed as follows:

$$\varepsilon = 100 - \frac{i_{loss}}{i_c} \times 100$$
$$= 100 - \frac{i_{loss,min}}{i_c} \times 100 - \frac{100}{i_c} \frac{zFD_{imp}}{\delta} \Delta c_{imp} \quad (16)$$

where i_c is the total cathodic current density.

The concentration of the reducible impurity species $M^{(x+z)+}$, or the change in the concentration over the diffusion layer, Δc_{imp}, may not be easy to obtain from experimental data. The total impurity concentration c_M, is more easily detected. It can be assumed that the concentration change of the reducible impurity species is roughly proportional to small variations of the total concentration of the impurity species:

$$\Delta c_{imp} \propto c_M \quad (17)$$

Equation 16 can then be written as

$$\varepsilon = \varepsilon_{max} - \frac{100}{i_c} B_M c_M \quad (18)$$

where ε_{max} is the CE corresponding to $i_{loss,min}$, and B_M is a proportionality constant. Plotting CE against impurity concentration should, according to Equation 18, give a straight line for a given cathodic current density.

The total effect of several different impurity species on CE is assumed to correspond to the total additive effect of each individual impurity species, which means that Equation 18 can be extended as follows:

$$\varepsilon = \varepsilon_{max} - \frac{100}{i_c} [B_1 c_1 + B_2 c_2 + \cdots + B_n c_n]$$
$$= \varepsilon_{max} - \frac{100}{i_c} \sum_1^n [B_n c_n] \quad (19)$$

The additive effect of impurities on CE will be investigated in the present work. Note that $i_{loss,min}$ and consequently ε_{max} depend on the k_{mix} value for $\delta_{mix} = \delta$. This means that ε_{max} will definitely decrease with increase in the convective flow in the system. The effect on CE will be partly counteracted by a corresponding decrease in impurity concentrations. The term behind ε_{max} in Equation 19 represents the 'excess loss' in CE due to cyclic redox reactions. If this end term becomes zero, then a shift in the rate determining step will take place as discussed above.

3. Experimental details

The laboratory cell and the experimental procedure were described previously [3]. The experiments were carried out at 980 °C and with a molar ratio NaF/AlF_3 equal to 2.5. The concentration of CaF_2 was 5 wt %, while the concentration of alumina was in the range 4 to 6 wt %. The total current applied was 26.54 A, corresponding to a cathodic current density, i_c, of 0.85 A cm^{-2}.

The concentration range of impurity species investigated in the present work are given in Table 1 together with corresponding mass transfer coefficients. The influence of various impurities on CE was originally studied with adding only one impurity to the cell with the alumina feed. The amounts added to achieve a certain concentration level were calculated by means of the mass transfer coefficients given in Table 1.

4. Results and discussion

The impurities studied may be categorized as: (i) impurities with roughly no effect on CE and (ii) impurities which lower the CE considerably with only small additions.

4.1. *Impurities with limited or no effect on CE*

The results from the study of CE with additions of MgF_2 and BaF_2 to the electrolyte are given in Table 2, together with CE data obtained with no impurity additions. The CE results when CuO, B_2O_3 and SnO_2 were added are given in Figs 3–5.

The cations of the species given in Table 2 are most probably present only with the oxidation state +2. They therefore do not participate in cyclic redox reactions in the electrolyte. The only influence of these species on CE may be due to (i) the effect these species have on the activities of NaF and AlF_3 in the electrolyte as discussed elsewhere [2, 4], and (ii) the effect due to codeposition with aluminium on

Table 1. Impurity compounds added to the electrolyte and investigated composition range of the cation, $M^{(x+z)+}$

Compound	$M^{(x+z)+}$/wt %	k_i^*/cm s^{-1}
MgF_2	0–0.05	–
BaF_2	0–0.24	–
ZnO	0–0.11	1.2×10^{-4}
Fe_2O_3	0–0.12	1.4×10^{-4}
P_2O_5	0–0.06	1.9×10^{-6}
$Ca_3(PO_4)_2$	0–0.06	1.9×10^{-6}
SiO_2	0–0.06	2.6×10^{-4}
V_2O_5	0–0.12	1.2×10^{-4}
TiO_2	0–0.10	1.9×10^{-4}
Ga_2O_3	0–0.15	3.0×10^{-4}
CuO	0–0.13	6.9×10^{-6}
B_2O_3	0–0.02	9.2×10^{-6}
SnO_4	0–0.25	1.9×10^{-5}

*k_i is the mass transfer coefficient.

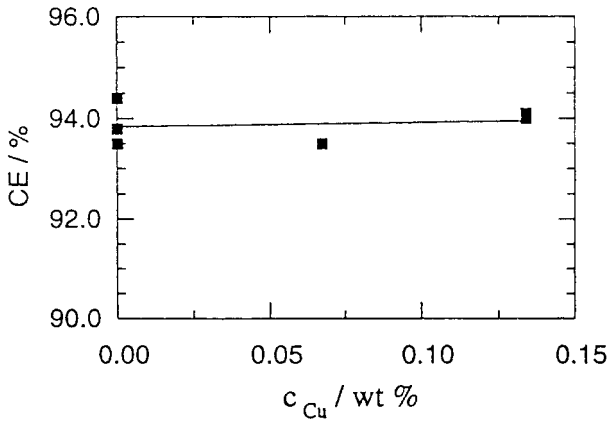

Fig. 3. CE as a function of the total electrolyte concentration of copper species, c_{Cu}.

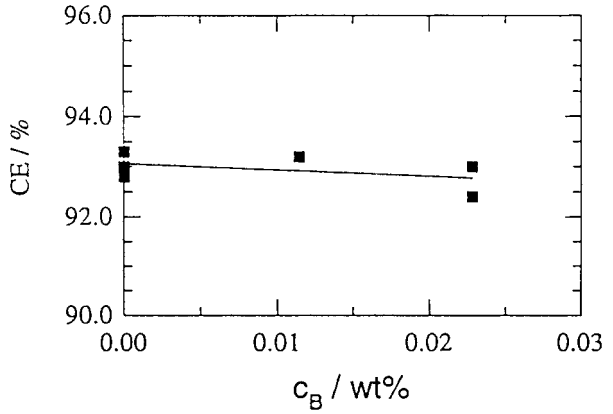

Fig. 4. CE as a function of the total electrolyte concentration of boron species, c_B.

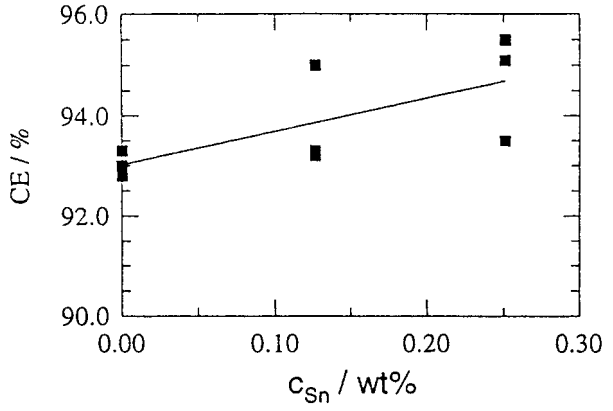

Fig. 5. CE as a function of the apparent concentration of tin ions in the electrolyte. The solubility limit was exceeded.

the cathode. These effects are important only at comparatively high concentrations of the added impurity.

The results shown in Figs 3 and 4 show that additions of CuO and B_2O_3 have little or no influence on CE, indicating that the corresponding ions do not participate in cyclic redox reactions. SnO_2, on the other hand, has an apparently positive effect on CE as shown by Fig. 5. However, the solubility of SnO_2 in the system is very low [16–18], probably less than

Table 2. CE without excess impurity additions and with additions of MgF_2 and BaF_2 to the electrolyte

Compound	$M^{(x+z)+}$/wt %	*CE*/%
–	–	92.8
–	–	93.3
–	–	93.0
MgF_2	0.05	92.9
MgF_2	0.05	93.2
BaF_2	0.24	93.2
BaF_2	0.24	93.5

0.02 wt % [18] for the present melt composition, which means that the solubility limit for SnO_2 has been exceeded. The apparent increase in CE found in the present investigation may thus be due to the following alloying reaction:

$$4Al(l) + 3SnO_2(s) = 2Al_2O_3(diss) + 3Sn(in\ Al) \quad (20)$$

taking place at the metal/electrolyte interface. If all the SnO_2 reacts according to Equation 20, an increase in CE according to the solid line in Fig. 5 is expected. The measured CE values are in agreement with the line, indicating that tin has entered the metal phase almost quantitatively.

4.2. *Impurities with detrimental effect on CE*

CE as functions of the concentration of the impurity species Fe, P, Si, V, Zn, Ti and Ga are presented graphically in Figs 6–12. The experimental data can be fitted to straight lines in agreement with Equation 18. The solid lines in the Figures are determined by regression analysis discussed below.

Impurity compounds with cations of the highest oxidation state were added in the present study. The effect that possible variations in the valence distribution of incoming impurity species may have on the loss in CE, can be estimated using iron as an example. With added Fe^{3+} corresponding to 0.12 wt % iron in the electrolyte, the change in CE was experimentally determined to be –2.8%. Assuming that Fe^{3+} initially

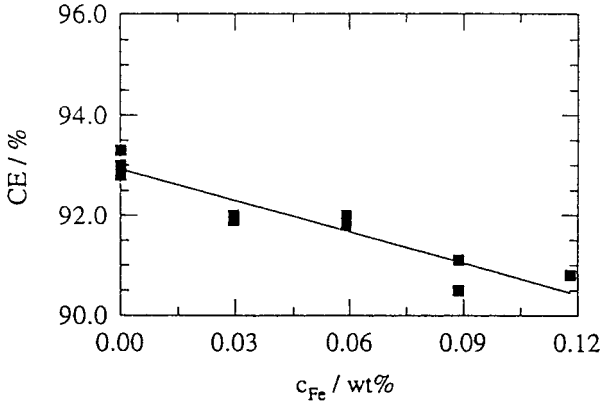

Fig. 6. CE as a function of the total electrolyte concentration of iron species, c_{Fe}. Regression line: $CE = (93.0 \pm 0.6) - (23.2 \pm 3.8)\ c_{Fe}$.

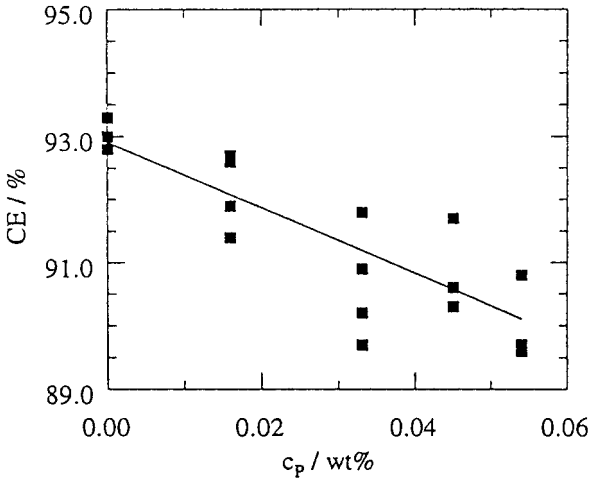

Fig. 7. CE as a function of the total electrolyte concentration of phosphorous species, c_P. Regression line: $CE = (93.0 \pm 0.6) - (67.8 \pm 18.4)c_P$.

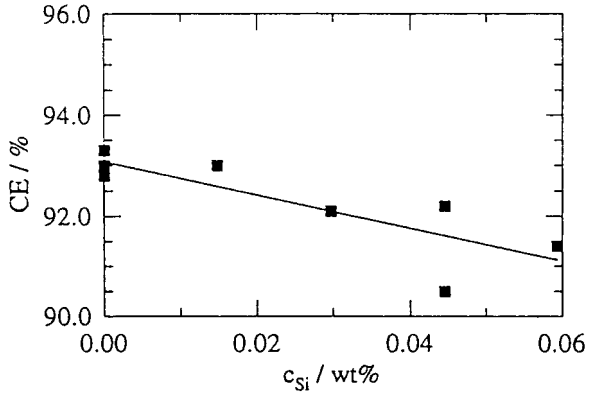

Fig. 8. CE as a function of the total electrolyte concentration of silicon species, c_{Si}. Regression line: $CE = (93.0 \pm 0.6) - (31.3 \pm 12.4)c_{Si}$.

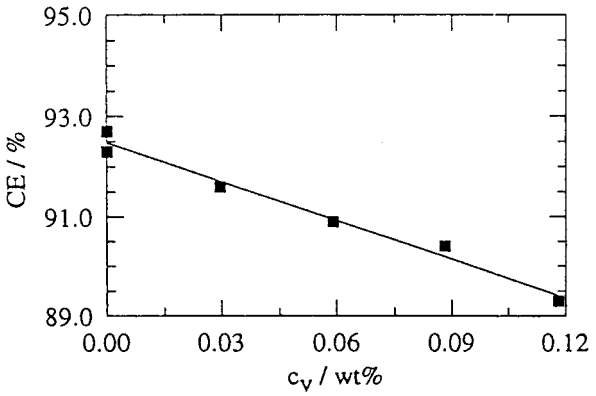

Fig. 9. CE as a function of the total electrolyte concentration of vanadium species, c_V. Regression line: $CE = (92.5 \pm 0.6) - (26.3 \pm 4.4)c_V$.

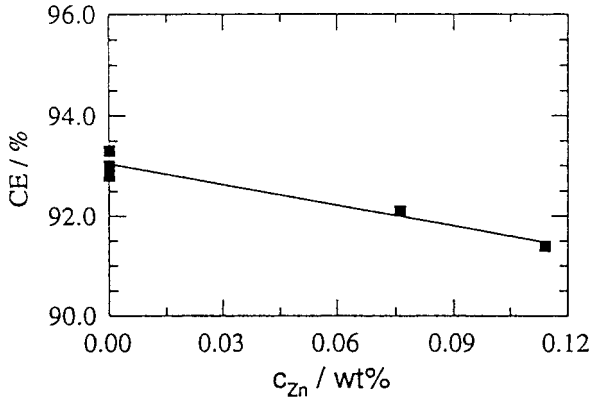

Fig. 10. CE as a function of the total electrolyte concentration of zinc species, c_{Zn}. Regression line: $CE = (93.0 \pm 0.6) - (13.4 \pm 3.2)c_{Zn}$.

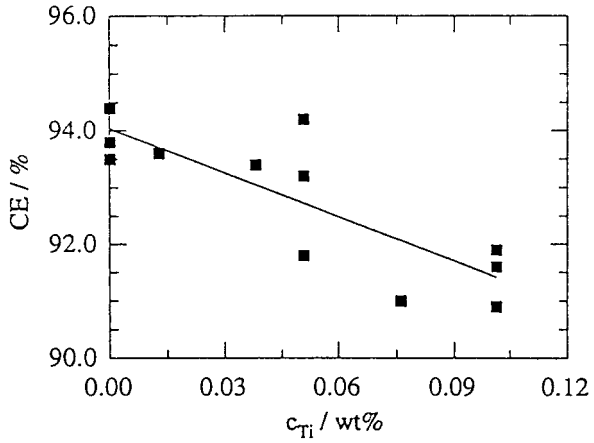

Fig. 11. CE as a function of the total electrolyte concentration of titanium species, c_{Ti}. Regression line: $CE = (93.9 \pm 0.6) - (24.2 \pm 13.2)c_{Ti}$.

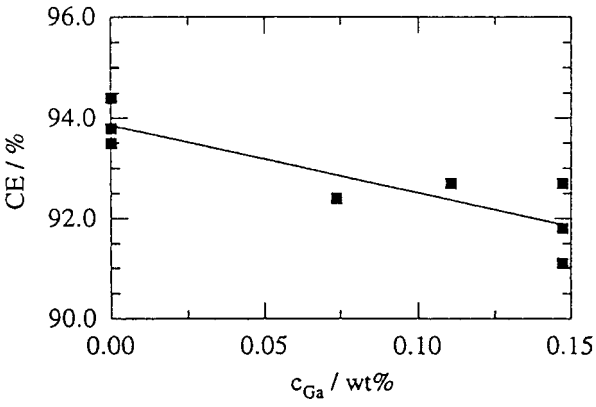

Fig. 12. CE as a function of the total electrolyte concentration of gallium species, c_{Ga}. Regression line: $CE = (93.9 \pm 0.6) - (13.8 \pm 7.6)c_{Ga}$.

reacts to a steady state valence distribution with 70% Fe^{2+} and 30% Fe^{3+}, then the consumption of RE corresponds to a reduction in CE of 0.15%. The valence distribution of the incoming impurity species can, from similar calculations, be considered to be of minor importance when discussing the results given in Figs 6–12.

If all the added Fe^{3+} reacts according to

$$Fe^{3+} + 3e^- = Fe(\text{in Al}) \qquad (21)$$

an apparent increase in CE should be expected if the deposited iron is included in the metal production. A hypothetical decrease in CE of about 0.7% can be calculated if that amount of iron is deposited but not included in the CE calculation. The only reasonable

explanation of the observed 2.8% decrease in CE shown in Fig. 6 seems to be some kind of cyclic redox reactions coupled to the loss process. Generally, the detrimental effect on CE with the impurities shown in Figs 6–12 can hardly be explained without including cyclic redox reactions.

4.3. *Uncertainty in CE and regression lines*

The experimental values for the CE without deliberate addition of impurities are not the same in all the Figs 3–12. The main reason for these deviations is probably that the various experiments were performed in time periods with slightly different impurity contents in the base electrolyte. The experiments were also performed in two different furnaces with a somewhat unavoidable difference in temperature distribution and cell hydrodynamics, giving somewhat different mass transfer coefficients and CE values.

The solubilities of Fe_2O_3 (0.003 wt %) in Na_3AlF_6 – 5 wt % Al_2O_3 and of ZnO (0.004 wt %) in Na_3AlF_6 – 5 wt % Al_2O_3 reported by Belyaev *et al.* [16], are considerably lower than found by other workers. De Young [19] found a solubility of Fe_2O_3 corresponding to 0.11 wt % Fe^{3+} cations in cryolite-based melts with 7wt % Al_2O_3 at 980 °C. Hayakawa and Kido [20] found a ZnO solubility in cryolite of 3.2 wt % at 1000 °C. With the exception of SnO_2, the solubility limits for the added oxides have probably not been exceeded in the present work.

The slope of CE as a function of the impurity content, $d\varepsilon/dc_i$, was calculated by a least square fit. The uncertainty in the slope was set equal to (±) twice the value of the calculated standard error. The results are given in Table 3. The equation for CE as a function of the Zn concentration was determined from rather few experimental values, see Fig. 10, and the real uncertainty in the coefficient $d\varepsilon/dc_{Zn}$ is probably higher than indicated in the Table.

The concentration of impurities given in Figs 6–12 corresponds to the initial amount of impurities deliberately added to the electrolyte. The rate of impurity transport into the metal and the gas phase in commercial cells was estimated from an extensive mass balance study [21]. The derived mass transfer coefficients (Table 2) were used to calculate the necessary impurity feed rate and the corresponding steady state concentration in the electrolyte.

Impurities will to some degree be codeposited and alloyed with aluminium. This can influence the CE determined from the amount of metal produced, especially if the codeposited impurity species has a high molar mass compared to aluminium. Calculations indicate that gallium is the only impurity among those investigated which may lead to a significant influence on CE. Deposition of gallium may increase CE by approximately 0.8% for the highest concentration shown in Fig. 12. If this is corrected for, the slope of CE as a function of gallium concentration on a molar basis should be roughly the same as the corresponding slopes for iron and vanadium illustrated by the lines in Fig. 13. However, the change in the valence state for the impurity species taking part in the redox reactions is not easily deduced from Equation 16 and the slopes given in the figure. The detrimental effect of phosphorous on CE may be related to several shifts in the valence state between +5 and 0 with corresponding consecutive cyclic redox reactions within the cathode boundary layer.

4.4. *Comparison with previous work*

Table 4 show less decrease in CE with increasing impurity concentrations, compared to previous work in laboratory cells [11, 13, 14]. The reason for this discrepancy may be related to differences in cell design and current density distribution.

4.5. *Additive versus nonadditive effect of impurity species on CE*

Assuming an additive effect of the individual impurities on CE, the following empirical equation was obtained:

Table 3. Calculated slope, $d\varepsilon/dc_i$, of current efficiency, ε/% with as a function of the concentration of various impurities, c_i/wt%

Uncertainty is set equal to twice the standard error.

Impurity	$d\varepsilon/dc_i$
Fe	−23.2 ± 3.8
P	−67.8 ± 18.4
Si	−31.3 ± 12.4
V	−26.3 ± 4.4
Zn	−13.4 ± 3.2
Ti	−24.2 ± 13.2
Ga	−13.8 ± 7.6

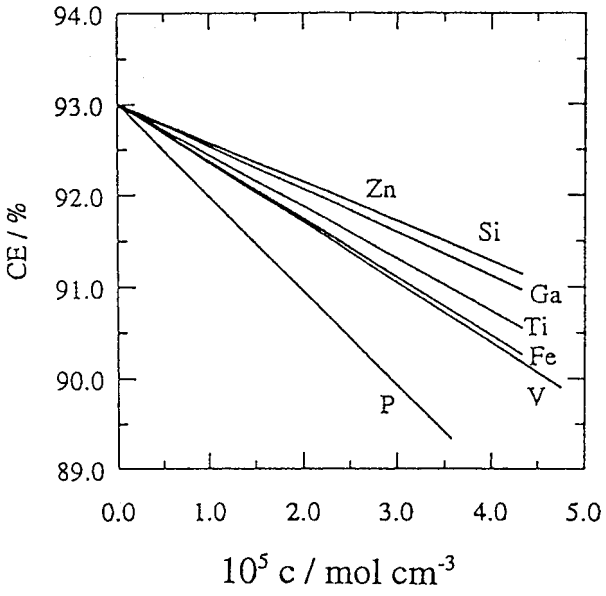

Fig. 13. CE as a function of the concentration of impurities (mol cm^{-3}), given as regression lines.

Table 4. Reduction in CE by addition of 0.01 wt % of impurity cations, ΔCE (percent): a comparison of the present work, ΔCE(1), with literature data, ΔCE(2)

Impurity	*ΔCE(1)*	*ΔCE(2)*	*Ref.*
Fe	0.23 ± 0.04	0.3	[13]
P	0.68 ± 0.18	0.95–1.0	[11, 13]
Si	0.31 ± 0.12	–	
V	0.26 ± 0.04	0.65–1.85	[13, 14]
Zn	0.13 ± 0.03	–	
Ti	0.24 ± 0.14	0.75	[13]
Ga	0.14 ± 0.08	1	[14]

$$\varepsilon = \varepsilon_{max} - \frac{100}{i_c}\,(0.197\,c_{Fe} + 0.576\,c_P + 0.266\,c_{Si} + 0.224\,c_V + 0.114\,c_{Zn} + 0.206\,c_{Ti} + 0.117\,c_{Ga}) \quad (22)$$

where c_i is the total concentration of the various impurity species given in wt % of cations.

The data in Fig. 14 show that the effect of a simultaneous addition of Fe and V is, within experimental uncertainty, equal to the sum of the individual effects predicted by Equation 22.

An electrolyte containing four different impurity species was composed as follows: 0.030 wt % Fe, 0.015 wt % Si, 0.014 wt % V and 0.013 wt % Ti. Two parallel experiments were carried out, with determined CEs equal to 89.8% and 91.7% . The average value of (90.8 ± 1.0)% compares well to the predicted CE value of 91.2% from Equation 22.

These results support the idea that the effects of individual impurity species on CE are approximately additive in the range of concentrations studied.

4.6. *Impurity contents of a laboratory electrolyte without added impurities*

The entire solidified electrolyte from an experiment with no impurities added ($\varepsilon = 93.0\%$), was thoroughly crushed and mixed. A sample was treated

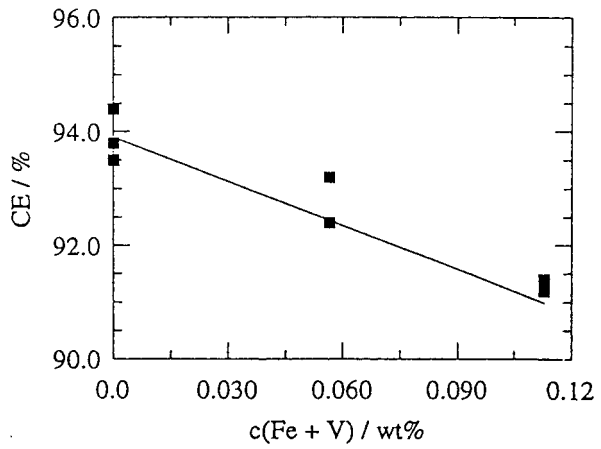

Fig. 14. CE as a function of the sum of Fe and V concentrations in the electrolyte. Equal molar concentrations of Fe and V were added to the electrolyte. Line: Equation 22.

Table 5. Analysis of a laboratory electrolyte without added impurities

Element	*Sample* 1/ppm	*Sample* 2/ppm
Fe	33.9	36.7
Ti	3.9	3.0
V	0.3	0.4

with HCl in a platinum crucible. Two parallel analyses of the aqueous solution were performed by an IC plasma spectrometry method. The results are given in Table 5.

The impurity concentrations in Table 5 give a CE value roughly 0.1% lower than ε_{max}, according to Equation 22. The concentrations of other impurities not analytically detected are probably small, which means that the CE values obtained in the present laboratory cell without impurity additions are close to ε_{max}.

5. Application of impurity CE model to commercial cells

The convective flow in the present laboratory cell is different from that in a commercial Hall–Heroult cell. However, the cathode concentration overvoltage and CE for a given current density in the two types of cells are roughly equal, when the magnetic fields in the commercial cell are well balanced [4]. This means that the thickness of the cathode boundary layer and the rate of mass transfer processes in the boundary layer should approximately be of the same size in the two types of cells. This means that Equation 22 may be roughly valid for modern commercial cells operating with CEs in the region 92 to 96% . The steady state concentration regions of impurity species in commercial cells are not well known, since few data are published [6–8]. Certainly, the concentration level of impurity species is higher in commercial cells than in the present laboratory cell during experiments with no impurity additions to the electrolyte. The results obtained with the present laboratory cell indicate that the loss in CE under all conditions studied can be related to cyclic redox reactions. This means that the loss in CE during normal operations of modern commercial cells operating with high CEs (94–96%) should be related to cyclic redox reactions [1–4] and not to the traditional 'back reaction',

$$2\text{'Al'} + 3CO_2 = Al_2O_3 + 3CO \quad (23)$$

where 'Al' is dissolved aluminium in the form of reduced entities, RE.

Some previously unpublished data [21] for impurity species in commercial cells are given in Table 6, together with calculated loss in CE from Equation 22 for individual ions. For the cell in question the excess loss in CE due to electrolyte impurities amounts to about 1% . It is evident from Equation 22 and the data in Table 6 that it is important to keep the elec-

Table 6. Electrolyte impurity levels in a commercial cell with prebaked anodes and estimated loss in CE due to each impurity element, ΔCE

Element	*c*/wt %	ΔCE/%
Fe	0.0174	−0.40
P	0.0072	−0.49
V	0.0011	−0.03
Si	0.0025	−0.08
Ga	0.0014	−0.02
Zn	0.0007	−0.01

trolyte impurity concentrations at a minimum level to reach a high current yield.

6. Concluding remarks

The results show a roughly linear decrease in CE with increasing electrolyte concentration of the polyvalent impurity species. The effects of the individual impurity species on CE appear to be approximately additive for electrolytes containing more than one impurity species like, Fe, Si, V and Ti. This influence of certain impurity species on CE is too large to be explained by a simple codeposition mechanism or a single reduction to lower valent soluble species. An appropriate mechanism fitting the observed decrease in CE is cyclic redox reactions in the cathode and anode/CO_2 boundary layers. Such a mechanism may also dominate in commercial cells, since impurity species are generally present at the same levels as in our laboratory cell.

Acknowledgements

Financial support from The Research Council of Norway and from Norwegian aluminium industry is gratefully acknowledged.

References

[1] Å. Sterten and P. A. Solli, *J. Appl. Electrochem.* **25** (1995) 809.
[2] *Idem, ibid.* **26** (1996) 187.
[3] P. A. Solli, T. Eggen, S. Rolseth, E. Skybakmoen and Å. Sterten, *ibid.* **26** (1996) 1019.
[4] P. A. Solli, T. Eggen, E. Skybakmoen and Å. Sterten *ibid.* **27** (1997) 939.
[5] H. G. Johansen, 'Jern som forurensningselement i aluminiumelektrolysen', Dr. ing. thesis, Department of Electrochemistry, Norwegian University of Science and Technology (NTH), Trondheim, Norway (1975).
[6] K. Grjotheim, C. Krohn, M. Malinovsky, K. Matiasovsky and J. Thonstad, 'Aluminium Electrolysis. Fundamentals of the Hall–Héroult process', 2nd. edn., Aluminium-Verlag, Düsseldorf (1982), Ch. 10.
[7] K. Grjotheim and K. Matiasovsky, *Aluminium* **59** (1983) 687.
[8] Å. Sterten, *Acta Chem. Scand.* **44** (1990) 873.
[9] Å. Sterten, 'Light Metals' (edited by E. L. Rooy), Proceedings of 120th TMS annual meeting, New Orleans (1991), p. 445.
[10] C. Szeker, *Acta Technika Acad. Sci. Hung.* **10** (1954) 19.
[11] A. Kerouanton and J. Badoz-Lambling, *Rev. Chim. Minerale* **11** (1974) 223.
[12] E. B. Frolova, V. B. Dobrokhotov, and A. M. Tsyplakov, *Trudy VAMI* **89** (1974) 36.
[13] J. Gerlach, and L. Deininger, *Metall.* **33** (1979) 131.
[14] N. I. Anufrieva, L. S. Baranova and Z. N. Balashova, *Sov. J. Non-Ferrous Met.* **24** (1983) 38.
[15] R. Keller, 'Light Metals' (editor J. E. Andersen), Proceedings of the 111th TMS annual meeting, Dallas (1982), p. 215.
[16] A. I. Belyaev, M. B. Rapoport and L. A. Firsanova, 'Elektrometallurgiya Alyuminiya', Metallurgizdat, Moscow, (1953).
[17] M. Rolin and C. Bernard, *Bull. Soc. Chim. Fr.* (1963), p. 1035.
[18] H. Xiao, J. Thonstad and S. Rolseth, *Acta Chem. Scand.* **49** (1995) 96.
[19] D. de Young, 'Light Metals' (editor R. E. Miller), Proceedings of the 115th TMS annual meeting, New Orleans (1986), p. 299.
[20] Y. Hayakawa and H. Kido, *J. Electrochem. Soc. Japan* **20** (1952) 263.
[21] P. A. Solli, 'Current Efficiency in Aluminium Electrolysis Cells', Dr. ing. thesis, Department of Electrochemistry, Norwegian University of Science and Technology (NTH), Trondheim, Norway (1993), p. 187.